Reduction of turbulent skin friction by microbubbles

N. K. Madavan, S. Deutsch, and C. L. Merkle
Applied Research Laboratory and The Department of Mechanical Engineeering, The Pennsylvania State University, State College, Pennsylvania 16801

(Received 10 September 1982; accepted 19 October 1983)

Measurements of the effect of microbubbles on a zero pressure gradient turbulent boundary layer generated on the test section wall of a water tunnel are described. Microbubbles are created by injecting air through a 0.5 μm sintered stainless steel plate immediately upstream of a floating element drag balance. At the downstream edge of the balance the length Reynolds number is as high as ten million. Integrated skin friction reduction of greater than 80% is observed. The drag balance results are confirmed by measurements with a surface hot-film probe. For the case in which buoyancy tends to keep the bubbles in the boundary layer, the skin friction data are shown to collapse when plotted against the ratio of air to water volume flow rate. The effects of buoyancy on skin friction reduction are also documented.

I. INTRODUCTION

Results of an experimental program directed towards assessing the effects of very small gas bubbles (microbubbles) on a liquid turbulent boundary layer are described. For the most part, the gas of interest is air, and the liquid is water. The experiments are stimulated by a desire to reduce the skin friction in a turbulent boundary layer. Although the results are encouraging, it is too soon to speculate if this technique is to have engineering benefits.

Microbubble drag reduction studies are perhaps an outgrowth of the age-old idea of placing a layer of air between a ship and its water boundary layer to reduce the skin friction. This idea was patented in the 1800's,[1] although its practicality seems highly improbable, if for no other reason than the instability of the air–liquid interface so generated. The use of very small bubbles eliminates this interfacial instability while retaining many of the benefits of the original concept.

The first experimental work with microbubbles was reported by McCormick and Bhattacharyya[2] in 1973. They used a copper wire wound around a towed body of revolution to produce hydrogen bubbles by electrolysis. The presence of pressure gradients and boundary layer transition on the body make it difficult to separate the effects of skin friction and form drag or to study the detailed mechanisms whereby the drag reduction was realized. In addition, the results were limited to Reynolds numbers between 0.3 and 1.8 million.

The effects of microbubbles on a turbulent boundary layer have also been studied by a group of Soviet scientists.[3–6] Instead of using electrolysis to generate the bubbles, they forced air through a porous surface with pore sizes ranging from 1 to 50 μm. Their experiments were conducted using a simple flat plate geometry and all measurements were made downstream of the porous section. The measurements included the local skin friction, the bubble concentration profiles, and portions of the velocity profiles. The results showed that the local skin friction could be reduced to nearly 10% of its undisturbed value by microbubble injection. The maximum skin friction reduction was observed to occur near the porous section while further downstream the boundary layer gradually relaxed back toward its undisturbed condition. The parameters that control the characteristic length that describes this relaxation were not determined, but are probably attributable to the migration of the microbubbles outside the boundary layer. Such migration could occur because of buoyancy, diffusion, or interaction with the local mean velocity gradient. It appears that the Soviet experiments were performed with the boundary layer above the porous surface so that the effect of buoyancy was to remove the bubbles from the boundary layer.

In contrast to the general result that microbubbles decrease the skin friction, it was noted[4] that at the lowest tunnel velocities a small concentration of bubbles caused the skin friction to increase slightly. Since the characteristics of the undisturbed boundary layer were not reported, a conclusive explanation for this observation cannot be given, but it is possible that the increase occurred because the bubbles tripped a laminar boundary layer.

The bubble-concentration measurements reported in Refs. 3–6 showed a peak at a y/δ location of about 0.1. The magnitude of the volumetric concentration at this peak was as high as 80%. Near the wall, and in the free stream, the bubble concentration was characterized by a falloff to zero. By taking advantage of the absence of bubbles near the wall, the Soviet researchers made some laser Doppler anemometer (LDA) measurements of the near-wall velocity profiles. Because the LDA signal became too weak for use at bubble concentrations exceeding 3%, they were able to measure out only to $U/U_\infty \simeq 0.4$–0.6 depending on the concentration distribution. These near-wall velocity measurements showed clear evidence of a reduction in velocity gradient at the wall as the airflow rate was increased. Further, skin friction estimates based on these slopes were in reasonable agreement with the more direct skin friction measurements alluded to earlier that were obtained with surface-mounted hot films,[3] and small, flush-mounted floating element balances.[4,5]

The bubble sizes that are generated as the air flows through the porous material represent an additional important parameter of the microbubble boundary layer. References 3–6 report bubble diameters ranging from submicron

 0031-9171/84/020356-08$01.90

size to as high as 50 μm. These estimates are based upon injection into quiescent water, and a breakup criterion suggested by Hinata and Ohki[7] which depends on the Weber number of the bubbles. Silberman[8] and Hughes *et al.*[9] have reported measurements of bubble injection from a single orifice into a flowing liquid and have noted that the diameter is independent of hole size and depends only on the ratio of the flow rates of the two streams. No conclusive data concerning the variation of bubble sizes from a porous material into a flowing liquid appear to be available.

The results described in the present paper are directed toward investigating the basic physics of a turbulent boundary layer saturated with microbubbles. The primary data reported herein are measurements of the integrated skin friction downstream of a porous air injection section as a function of airflow rate and the free-stream velocity. Data are presented for three different plate orientations with respect to gravity, for two porous-section sizes, and for helium as well as air. Some local skin friction measurements at a single point on the surface are also reported. Auxiliary measurements include LDA surveys to document the characteristics of the undisturbed boundary layer into which the bubbles are injected, plus a few mean flow measurements in the outer part of the boundary layer in the presence of bubbles.

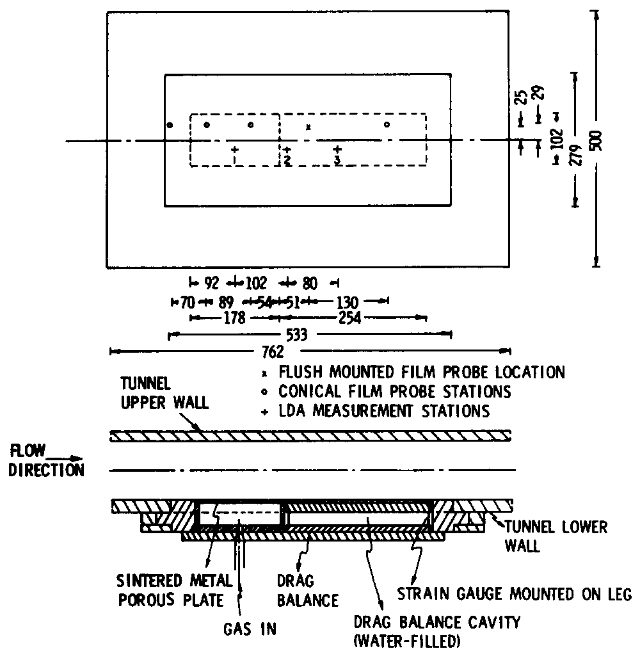

FIG. 1. Schematic of experimental setup showing location of hot-film and LDA measurement stations. (Diagram not to scale.)

II. EXPERIMENTAL FACILITY

The experiments were conducted at The Pennsylvania State University, in a water tunnel at the Applied Research Laboratory. The rectangular test section has dimensions of 508 mm $\times$ 114 mm $\times$ 762 mm long. Both tunnel velocity and pressure are continuously controllable, with a maximum test section velocity of about 25 m/sec and tunnel pressures ranging between 0.2 and 4 atm. The test section can be rotated at 90° intervals to allow buoyancy effects to be studied. In addition, a 0.2 m^3/sec bypass (roughly 15% of the tunnel volume flow rate at maximum speed) can be employed to keep the tunnel relatively air-free. Tunnel turbulence control is through a 152 mm section of honeycomb with a 25 mm core size and a 9:1 contraction section. The free-stream turbulence intensity was measured to be 0.3%–0.5% over the velocity range of interest.

The flat plate on which the measurements were performed was mounted in one wall of the rectangular test section in a 279 mm wide $\times$ 533 mm long opening intended for a window. Centered spanwise on the test plate was a 102 mm $\times$ 178 mm porous sintered stainless-steel section for gas injection, followed by a 102 mm $\times$ 254 mm force balance, as shown in Fig. 1. The sintered stainless-steel section is manufactured by Mott Metallurgical Corp. for use as a filter. The filter type chosen will trap particles of diameter 0.5 μm and larger. This corresponds to a nominal pore size of about 5.0 μm. An appropriate roughness height for the sintered porous material is 1.6 μm, as estimated by comparison with surface roughness gauges.

III. INSTRUMENTATION

The floating-element force balance used for the skin friction measurements employed a strain-gauged tension/compression member to infer integrated skin friction on the surface. Clearances around the balance, in the absence of flow, were nominally 0.038 mm at the leading edge, 0.25 mm at the trailing edge, and 0.10 mm on either side. Sealing around the force balance was avoided by filling the cavity underneath the balance with water, as shown in Fig. 1. Calibration of the force balance was performed by placing the entire test section window, with the porous and force-balance sections in place, horizontally on a table and using a pulley and weights arrangement. The balance showed excellent linearity to an applied force of ten newtons (corresponding to the turbulent shear force produced at a free-stream velocity of 18 m/sec). The calibration was used to convert the output voltage of the balance to force units. The force-balance output voltage was measured repeatedly at various stages of the tests as a function of water velocity (in the absence of microbubbles) to verify that the calibration remained unchanged. Throughout the tests, the force measurements with and without microbubbles were very repeatable.

The test section velocity was determined from the pressure drop across the tunnel contraction section. The transducer used for this purpose was calibrated before and after the experiments. Simple single-point checks were also employed during the runs.

Injected gas flow rates were measured with a turbine flow meter. Factory calibration of the turbine meter was assumed valid. Comparison of the turbine meter data with that from a rotameter indicated that this assumption was reasonable.

Tunnel velocity, integrated skin friction, gas pressure, and gas volumetric flow rate were visually monitored on integrating digital voltmeters and simultaneously recorded on two Nicolet Model 206 digital oscilloscopes. The digital readout of the tunnel velocity was used manually to maintain constant tunnel speed during the run. The oscilloscopes performed an analog-digital conversion and stored the data on floppy disks. Each channel of the oscilloscope has a storage capacity of 2048 points. Data were normally taken at the rate of five points per second, so that run times were approximately seven minutes in duration. During a run, the skin friction was first measured with no airflow. The airflow was then increased to its maximum value while taking data to the five-point-per-second rate. After reaching maximum flow rate, data taking was continued while the flow was again reduced to zero. Inspection of the data indicated excellent agreement between the data taken while the airflow was increasing and decreasing. The skin friction showed excellent repeatability in returning to its original zero-airflow value. Data reduction and analysis were performed on an IBM 3033. Data points for which the velocity varied by more than $\pm 1\%$ from the mean were excluded.

Local skin friction was also measured at a single location on the plate as shown in Fig. 1. A TSI Model 1471-W surface mounted hot-film probe and a DISA 55M01 anemometer were used for the measurements. (These flush-mounted hot-film data were recorded on the Nicolet and computer-linearized whereas the conical probe data described later were linearized by means of an analog device and recorded manually.) Time averaged values of the local shear stress were deduced from Nicolet records which were recorded at the rate of 20 000 points per second, allowing a record length of about 0.1 sec. Repeatability checks at constant tunnel conditions indicated that this record length was sufficient to resolve the mean skin friction. In addition to these short time records, some long time records (aproximately five minutes) were recorded on a Spectral Dynamics Model 360 Digital Signal Processor and used to obtain spectral information on the local shear stress.

The calibration of the hot film was based upon the characteristics of a flat plate boundary layer. The output from the hot film was measured as a function of free-stream velocity in the absence of microbubbles. These voltages were then related to the local skin friction by using the measured integrated skin friction on the plate and classical turbulent boundary layer correlations. The virtual origin used in these calculations were determined from the integrated skin friction measurements and the velocity profile measurements described later.

In addition to the skin friction measurements, the velocity and turbulence intensity profiles of the boundary layer into which the microbubbles were injected were surveyed by means of an LDA. To achieve a reasonable proximity to the test plate, the laser beams were directed through a sidewall window of the test section, at an angle of 8.8 deg to the test plate surface. This angle was necessitated by tunnel configurational constraints. Some preliminary surveys were also conducted using a conical hot-film probe and the LDA with the beams directed normal to the test plate surface. The achievable proximity to the wall in these preliminary surveys was limited. (The conical probe was limited by probe size, while the LDA was limited by wall reflections.) In addition to surveying the boundary layer without microbubbles, preliminary surveys with low concentrations of microbubbles present were also conducted.

The LDA measurements were taken with an 8 W argon ion laser and a TSI Model 1980 counter processor. Backscattering optics were employed with a $3.75\times$ beam expander and a 480 mm transmitting lens, providing an ellipsoidal sampling volume of 80 μm in the vertical and streamwise directions and 580 μm in the cross-flow direction. Positioning in the boundary layer was accomplished using an NRC Model 280 precision jack and monitored by a dial gauge with 25.4 μm gradations. The LDA data acquisition and reduction was performed on a minicomputer interfaced to the LDA counter processor. Output was presented on a video screen in the form of a histogram for each measurement point in the boundary layer. The mean velocity, turbulence intensity, and percent of samples retained in the calculations (a rough indication of the signal-to-noise ratio) were also printed on the screen. A correction to the LDA turbulence intensity measurements was obtained by matching the free-stream value to that measured by the conical hot-film probe. This correction was then applied to each point in the turbulent intensity profile.

Since the LDA velocity profiles were not recorded on the Nicolet oscilloscopes, manual control of the mean velocity should be taken to imply control to better than 1.5% without bubble injection and no more than 5% for the measurements with bubble injection.

IV. CHARACTERIZATION OF THE UNDISTURBED BOUNDARY LAYER

The static pressure distribution in the tunnel was measured at ten locations along the length of the test section using flush-mounted surface taps on the tunnel wall opposite the test plate. The measurements, shown in Fig. 2, indicate that the pressure varied by less than $\pm 0.7\%$ of the dynamic head over the length of the test section. No trends in the data are apparent. With the maximum flow rate of bubbles, the pressure at any given tap changed by less than $\pm 0.25\%$. If this entire variation were interpreted as an imposed pressure gradient acting on the plate, the corresponding pressure loading would change the observed amount of drag reduction by some 10%.

Mean velocity and turbulence intensity profiles were measured at three streamwise stations (as shown in Fig. 1) using the LDA. Measurements were made at each station at free-stream velocities of approximately 4.7 and 10.6 m/sec. The data are presented in inner variables in Fig. 3 and are seen to fit the law of the wall,

$$u^+ = A \log_{10} y^+ + B\,, \tag{1}$$

reasonably, where $A = 5.62$ and $B = 5.0$ have been chosen in accordance with the 1968 Stanford Conference.[10] The value of local skin friction obtained from the mean velocity profiles agreed reasonably well (within 6%) with the value predicted by classical boundary layer correlations.

Figure 4 shows the mean velocity profiles at free-stream velocities of 4.7 and 10.6 m/sec on u/U_∞ vs y/δ^* coordinates, where δ^* is the local displacement thickness. Purtell, Klebanoff, and Buckley[11] note that any underdevelopment

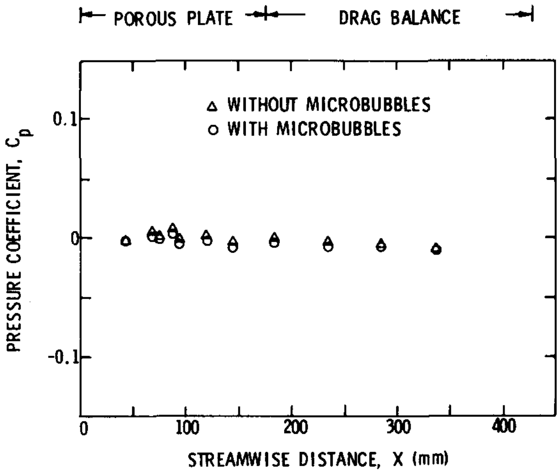

FIG. 2. The mapping of the pressure gradient along the test section. The distance X is measured from the leading edge of the porous plate.

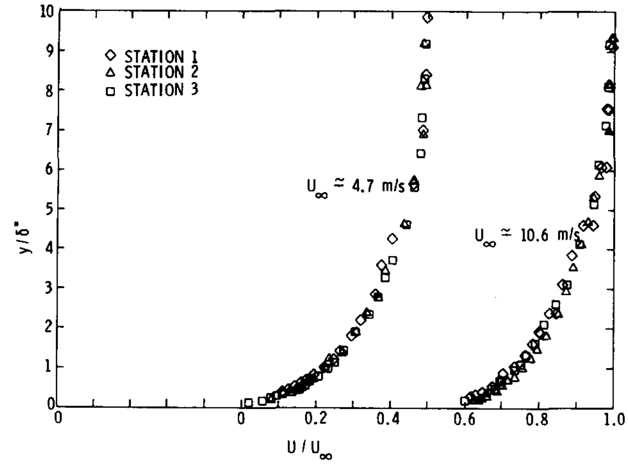

FIG. 4. The LDA velocity profile measurements in the absence of microbubbles presented in the outer variables. The location of measurement stations is noted in Fig. 1.

is more easily discernible in the outer region of the flow on a plot of this type. The experimental data at the different stations are seen to collapse to a single line for both free-stream velocities. The slight scattering in the higher speed data is primarily due to a drift in tunnel velocity which occurs at this speed during the prolonged periods of time (as much as five hours) required for completing these measurements. These results suggest that the boundary layer is "developed" in the sense of Coles.[12]

Turbulence intensities corresponding to the mean profiles are shown in Fig. 5.

Some representative measurements of integrated skin friction in the absence of microbubbles are given in Fig. 6 as a function of Reynolds number. These measurements were made on various occasions during the course of the experiments. The results show reasonable agreement with classical boundary layer data.[13]

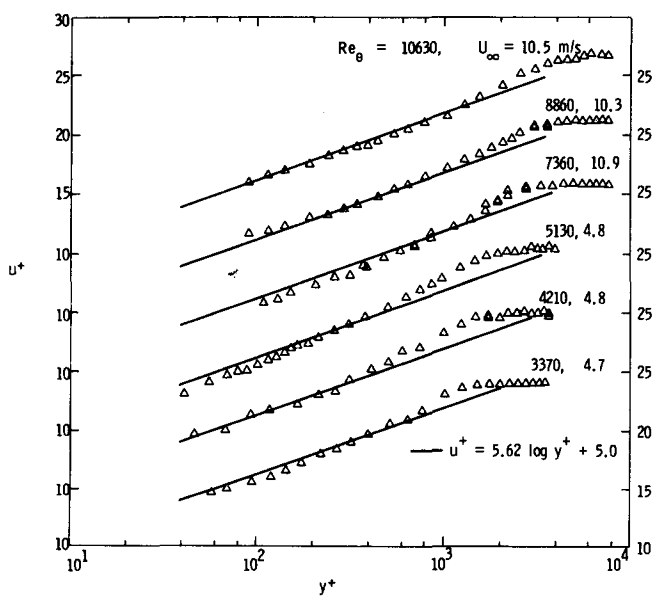

FIG. 3. The LDA velocity profile measurements in the absence of microbubbles presented in inner variables. Note the shifted origins.

V. RESULTS AND DISCUSSION

A. Integrated skin friction measurements

Integrated skin friction measurements were obtained for tunnel velocities ranging between 4.2 and 17.4 m/sec. This corresponds to length Reynolds numbers betwen 2.2 and 10.6 million at the downstream edge of the metric section. The corresponding Reynolds numbers at the upstream end of the porous section are 0.7 and 3.0 million. These Reynolds numbers are based on a fictitious boundary layer origin 180 mm upstream of the porous section. The origin was inferred from the boundary layer profile measurements.

The airflow rates used to generate the microbubbles ranged as high as 5×10^{-3} m^3/sec. On the basis of airflow per unit width of porous surface, these values are some five times larger than the maximum rates used in Refs. 3–6.

As stated previously, 2048 data points were taken in each run at a rate of five points per second. During this time, the tunnel velocity was held constant while the airflow was slowly varied from zero to the maximum and back to zero again. Two independent methods were used for evaluating the data comprising each constant velocity run. In the first procedure 50 data points were sampled at random from the complete set. This method gave a good representation of the

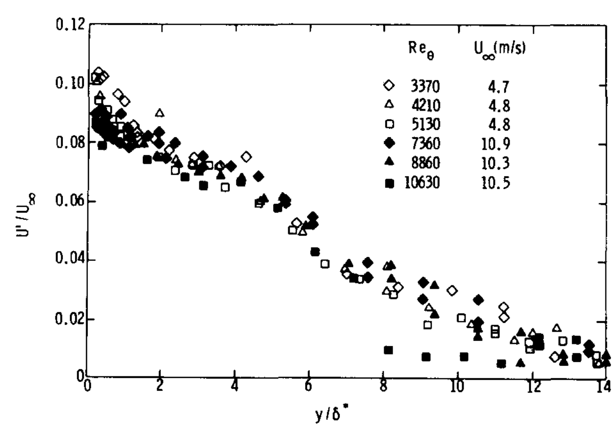

FIG. 5. The LDA data of turbulence intensity in the outer part of the boundary layer.

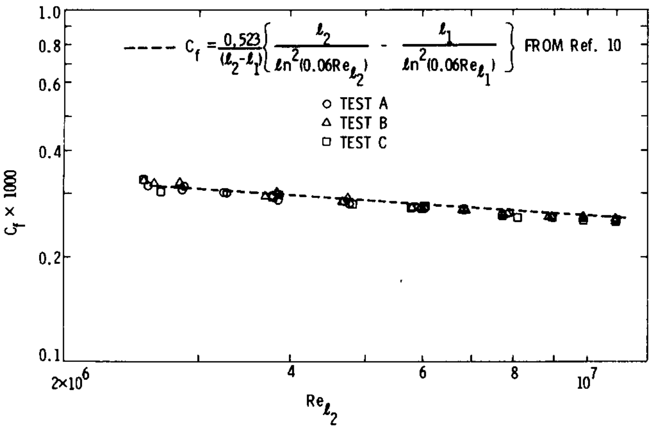

FIG. 6. Comparison of integrated skin friction measurements with classical boundary layer data. The symbols l_1 and l_2 denote distances to upstream and downstream edge of force balance, respectively, from virtual origin (356 and 610 mm).

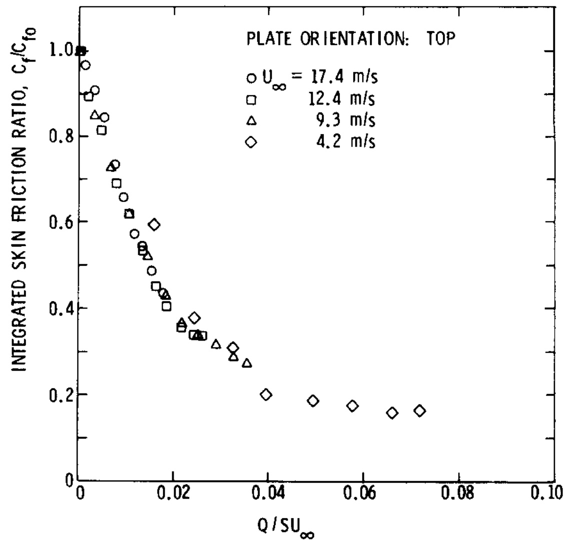

FIG. 8. Dimensionless skin friction as a function of dimensionless injection rate. The plate is above the boundary layer.

skin-friction/airflow behavior, but it gave limited information as to the expected data scatter. To remedy this, the second method was used. In this method the data were grouped into specified airflow intervals or bins and the data in each bin was averaged to find the mean data line. Bins were spaced evenly in 0.5×10^{-3} m^3/sec airflow intervals with widths of 0.025×10^{-3} m^3/sec. Confidence levels in each bin were determined by the Student T or F test. Bin populations ranged between 10 and 100 samples. The average curve as determined by this latter method was in excellent agreement with that obtained by the former.

The effect of microbubbles on the integrated skin friction for the case where the plate is on the top of the tunnel is given in Figs. 7 and 8. In this configuration, buoyancy tends to retain the bubbles in the boundary layer. Figure 7 shows that for all velocities the skin friction begins decreasing as soon as the airflow is turned on and continues to do so until, at the higher airflow rates, it approaches a constant minimum value. At the lower tunnel velocities the skin friction decrease is more pronounced because a given amount of airflow corresponds to a larger volumetric concentration of air in the boundary layer than at the higher speeds. The maximum observed skin friction reduction was in excess of 80% (see Fig. 7) and occurred at a tunnel velocity of 4.2 m/sec and an airflow of 4.0×10^{-3} m^3/sec.

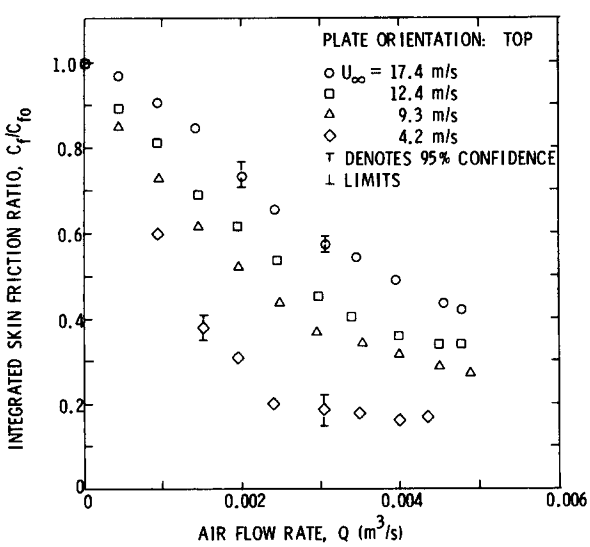

FIG. 7. Ratio of integrated skin friction in the presence of microbubbles to skin friction without microbubbles as a function of airflow rate. The plate is above the boundary layer.

In Fig. 8, the C_f/C_{f0} ratio for data taken with the plate on top is plotted against the nondimensional variable Q/SU_∞, where Q is the gas flow rate, U_∞ is the tunnel speed, and S is a reference area. For the present figure, this area has been taken as that of the wetted surface of the porous section. Note that this choice implies that Q/SU_∞ is the ratio of the effective velocity of the incoming air to the tunnel velocity. (Perhaps a better choice would be the cross-sectional area of the boundary layer, the displacement thickness times the width, in which case the nondimensional ratio would compare the volumetric flux of air to the volumetric flux of water in the boundary layer.) This parameter collapses the data for the plate on top to a single line that indicates a unique skin friction correlation for all tunnel speeds.

The results plotted in Fig. 9 represent two types of variations: data taken with helium as the injected gas, as well as data taken with airflow through only the downstream half of the porous section. The helium and half-porous section data also collapse quite reasonably when presented in terms of Q/SU_∞. The collapse of the helium data indicates that it is the volumetric concentration of the microbubbles, and not their mass concentration, which is the relevant parameter. Thus, the momentum of the incoming gas (which is nearly an order of magnitude smaller for helium than for air) does not appear to be a parameter. The collapse of the half-plate data (the same area was used in Q/SU_∞ for the half-plate as for the full plate) indicates that the area through which the bubbles are injected is not particularly important, but again that it is the volumetric flow rate.

The skin friction measurements for the two other plate orientations are given in Figs. 10 and 11 along with a comparison to the data for the plate on top. The comparison at

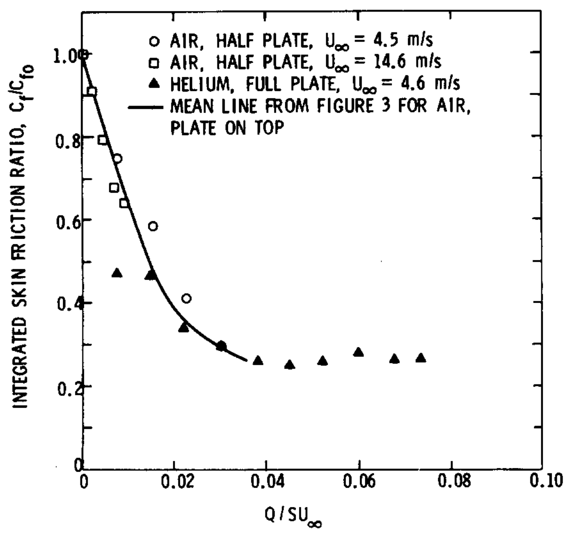

FIG. 9. Comparison of the effects of using helium instead of air as the injectant, and of using only half the porous plate. The plate is above the boundary layer.

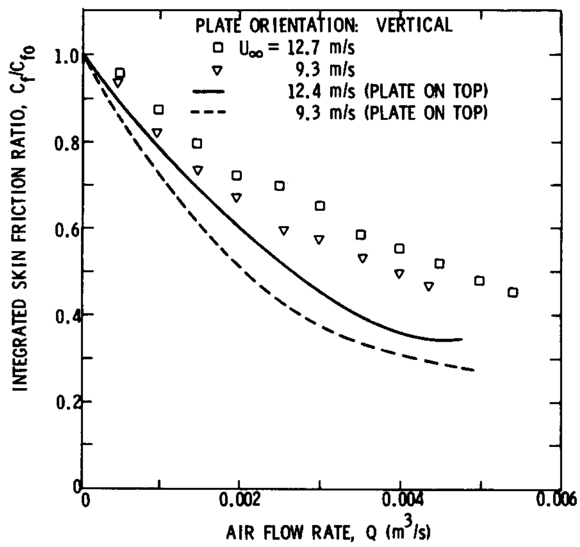

FIG. 11. The effects of buoyancy on skin friction reduction. Comparison of data taken with plate on top and with plate vertical (alongside the boundary layer).

the lower speed (9.3 and 9.6 m/sec) clearly shows that buoyancy effects are present. In particular, the results show that the skin friction reduction is considerably less than with the plate on top. Direct comparison at higher velocities is not available, but indications are that the effects of buoyancy are smaller at higher speeds.

The effects of buoyancy appear to be somewhat stronger when the plate is vertical than when it is on the bottom of the boundary layer. An interesting phenomenon was observed at low speeds (<2.5 m/sec) with the plate in the vertical position. The bubbles would remain spread out and close to the surface with seemingly little buoyancy effect for a while. Then, suddenly the entire gas "film" would roll up into a convoluted surface, which was highly buoyant, and would be swept up and away from the force balance. When this rollup occurred, the skin friction would immediately return to its gas-off value. These rolled-up and dispersed bubble configurations appeared to be bi-stable and one configuration would instantaneously change to the other for no apparent reason. This phenomenon was not observed at tunnel speeds above 2.5 m/sec.

B. Local skin friction measurements

The local skin friction, as measured with the flush-mounted hot-film probe at the position shown in Fig. 1, is presented in Fig. 12. These data were taken with the plate on the bottom. The local skin-friction reduction for a given airflow exceeds that obtained with the integrated measurements as can be seen by comparison with Fig. 10. This is to be expected, because the hot-film probe is relatively close to the porous injection plate so that the microbubbles have had little time to escape from the boundary layer. For these data, microbubble impingement on the hot-film probe was never

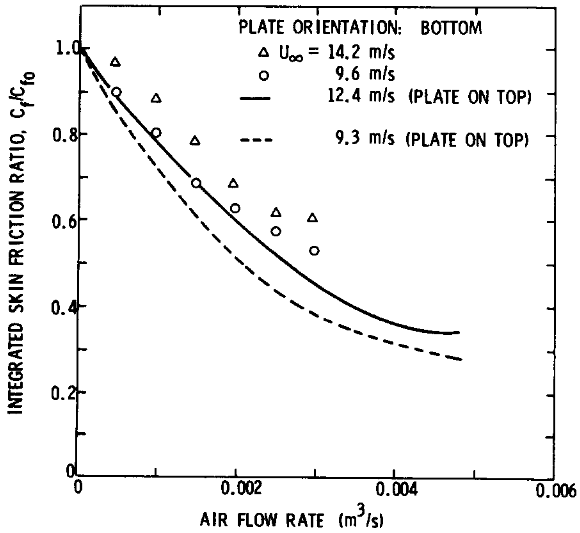

FIG. 10. The effects of buoyancy on skin friction reduction. Comparison of data taken with plate on top and plate on bottom.

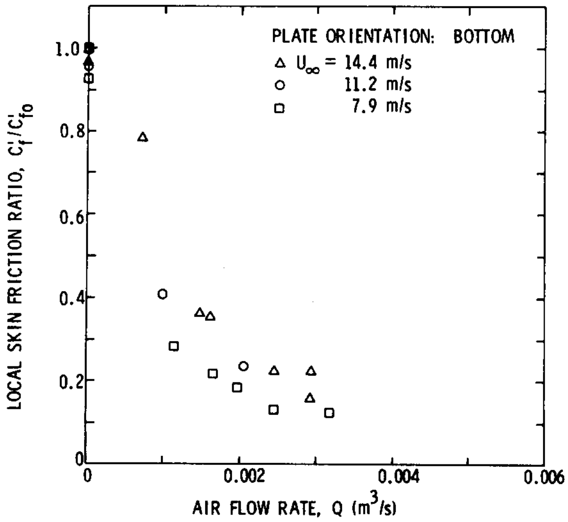

FIG. 12. Local skin friction as measured with surface-mounted hot film. The position of the gauge is noted in Fig. 10. The plate is on the bottom of the tunnel.

observed, whereas for the conical probe in the boundary layer, bubble impingement was detected fairly often. This is in agreement with earlier observations[5] that a bubble-free region exists close to the wall when the plate is on the bottom.

The oscilloscope trace of the flush-mounted hot-film probe also showed that the microbubbles decreased the high-frequency content substantially in comparison with the undisturbed boundary layer. This loss of high-frequency information in the presence of microbubbles was confirmed quantitatively from spectra taken on the frequency analyzer. The loss of high-frequency scales suggests a decrease in the turbulent Reynolds number such as would be generated by the increase in viscosity and decrease in density expected from the bubbles.

A comparison of LDA mean velocity profiles taken with and without microbubbles is given in Fig. 13. These data, taken at a free-stream velocity of 7.5 m/sec and an airflow rate of 0.5×10^{-3} m^3/sec and the LDA beams directed normal to the test plate, indicate a slight broadening in the velocity histogram when bubbles are present because of the introduction of more low-speed data points. (This broadening could have arisen because of scattering from large bubbles that were lagging the local mean velocity.) As can be seen, the presence of the microbubbles certainly causes no dramatic realignment of the characteristics of the outer boundary layer. Instead the velocities appear to be somewhat lower than they were in the absence of bubbles (as would be expected for a weaker gradient at the surface), but otherwise are nearly unchanged. Qualitative data taken with the conical hot film probe also showed the same trends.

VI. A POTENTIAL MECHANISM FOR THE EFFECTS OF MICROBUBBLES

The specific mechanisms by which microbubbles affect skin friction are a matter of conjecture, and must remain so until more detailed experimental evidence is available. Still, from the experimental data presented here and in the references, a possible mechanism similar to that acting in polymer solutions[14] begins to suggest itself, while another mechanism, boundary layer separation, may be ruled out.

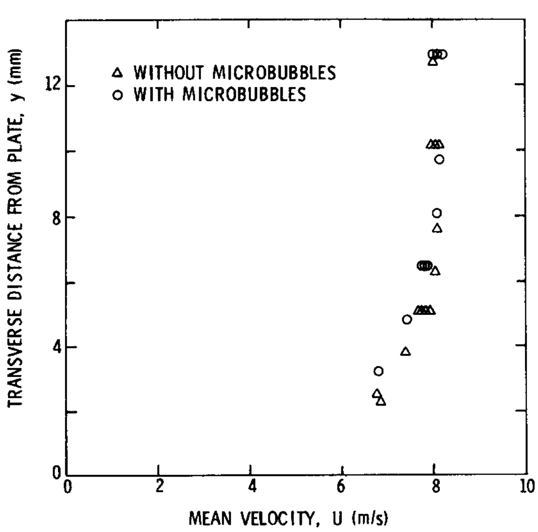

FIG. 13. Comparison of mean velocity profiles in outer part of boundary layer in the presence of microbubbles and in the absence of microbubbles.

Oral presentation of this material has raised the issue that the observed effects may be due to boundary layer separation. The presence of separation requires a reason: an adverse pressure gradient, removal of streamwise momentum, or addition of normal momentum. Figure 2 shows no evidence of an adverse pressure gradient. To be sure this is the pressure on the opposite wall, but C_f reduction of the magnitude noted here would be expected to have some effect on the opposite wall. Further, LDA measurements of the free-stream velocity over the force balance show no change when bubbles are injected. With regard to momentum changes, there is no mechanism whereby streamwise momentum can be removed from the flow; there is no place for a force to act. The injected air does add normal momentum, but its level is more than three orders of magnitude less than that required to separate a boundary layer.[15,16] The bubbles, which serve as an effective visualization device, provide more direct evidence that separation does not occur. Every visual evidence is that the microbubble boundary layer remains strongly attached and flat-plate-like in character. In addition, hot-film traces show no indication of the violent fluctuations which would be associated with a boundary layer near separation.

The mechanism leading to polymer drag reduction have been described by Lumley.[17,18] Briefly, outside the viscous sublayer of a high Reynolds number turbulent boundary layer, the rotation and strain rate fields are uncorrelated. Polymer molecules found there will stretch, resulting in increased solution viscosity. This additional viscosity (or decreased Reynolds number) will increase the size of the smallest eddies capable of surviving. Just outside the sublayer (the buffer region) where Reynolds stress-producing eddies are roughly the size of the Kolmogorov eddies, the turbulence is dissipated. The sublayer thickness increases and the skin friction is reduced. The same case can be made for certain types of particles in the flow.[17]

In the case of microbubble injection, the viscosity in the sublayer is unaffected because of the absence of bubbles there. Outside this region the bubbles cause both an increase in the absolute viscosity through an Einstein-type relation (say) and a decrease in the solution density. Again, this results in a thicker sublayer. The suggested mechanism offers a path whereby sizable skin friction reductions can be realized without postulating the presence of separation.

VII. CONCLUSIONS

The effects of injecting a high concentration of microbubbles into a turbulent boundary layer have been studied experimentally. The microbubbles were generated by injecting air (or helium) through a sintered stainless steel porous section with a nominal pore size of 5.0 μm. Instrumentation included a floating-element force balance 254 mm in length that was situated immediately downstream of the porous section, and a flush-mounted hot-film probe 51 mm downstream of the trailing edge of the injection section. The characteristics of the boundary layer into which the bubbles were injected were surveyed with a LDA and a conical hot film probe. The results showed that the integrated skin friction was reduced for all airflow rates and tunnel velocities. Maximum reductions of more than 80% were observed. With the plate on top of the tunnel, the ratio of the skin friction in the presence of microbubbles to that without microbubbles could be collapsed to a single curve by nondimensionalizing the volumetric airflow rate by the water velocity and an appropriate area. This same collapse of data could not be obtained with the plate on the bottom of the tunnel because in this orientation the effects of gravity enter as an additional parameter. With the plate on the bottom, the data at the lower tunnel speeds indicate that the reduction in skin friction was substantially less than was observed with the plate on the top. At the higher speeds, the effects of gravity are smaller. This indicates that the present tests nearly spanned the domain in which buoyancy effects are and are not significant for the present force balance length, tunnel speeds, and range of bubble sizes.

Local skin-friction measurements with the flush-mounted hot-film probe were in qualitative agreement with these integrated skin friction data. Spectra from the hot-film probe show that the presence of microbubbles causes a shift of the turbulence energy toward lower frequencies suggesting a reduction in the turbulent Reynolds number. The oscilloscope trace of the hot film showed no evidence of gas bubble impingement, supporting the notion of a bubble-free layer near the wall.

Velocity and turbulence intensity profiles in the outer region of the boundary layer show no dramatically different character when microbubbles are present as compared to when they are absent. This lends credence to the concept of a boundary layer modified by the presence of microbubbles as opposed to a complete restructuring of the flow field when the microbubbles are introduced.

Finally, we note that overall the present results are in qualitative agreement with earlier experiments.[3–6] Several parameters have been varied over wider ranges, and effects of gravity have been documented for the first time.

ACKNOWLEDGMENT

This work was sponsored by the Office of Naval Research under Contract No. N00014-81-K-0481.

[1]P. R. Crewe and W. J. Eggington, Trans. Roy. Inst. Nav. Arch. **102**, 315 (1960).

[2]M. E. McCormick and R. Bhattacharyya, Nav. Eng. J. **85**, 11 (1973).

[3]Yu. N. Dubnischev, E. R. Evseev, V. S. Sobolev, and E. N. Utkin, J. Appl. Mech. Tech. Phys. **16**, 114 (1975). Translated from Zhur. Prikl. Mekh. Tekh. Fiz. **1**, 147 (1975).

[4]G. S. Migirenko and A. R. Evseev, *Problems of Thermophysics and Physical Hydrodynamics* (in Russian) (Novosibirsk, Nauka, 1974).

[5]V. G. Bogdevich and A. G. Malyuga, in *Investigations of Boundary Layer Control* (in Russian), edited by S. S. Kutateladze and G. S. Migirenko (Thermophysics Institute Publishing House, Novosibirsk, 1976), p. 62.

[6]V. G. Bogdevich and A. R. Evseev, in *Investigations of Boundary Layer Control* (in Russian), edited by S. S. Kutateladze and G. S. Migirenko (Thermophysics Institute Publishing House, Novosibirsk, 1976), p. 49.

[7]S. Hinata and M. Ohki, Bull. Jpn. Soc. Mech. Eng. **14**, 951 (1971).

[8]E. Silberman, in *Proceedings of the Fifth Midwestern Conference on Fluid Mechanics* (University of Michigan, Ann. Arbor, MI, 1957), p. 263.

[9]N. H. Hughes, M. M. Reischman, and J. M. Holzmann, in *Proceedings of the Sixth Biennial Symposium on Turbulence* (University of Missouri, Rolla, MO, 1979), p. 274.

[10]D. E. Coles and E. A. Hirst (editors), *Proceedings of the* AFOSR-IFP-*Stanford Conference on Computation of Turbulent Boundary Layers* (Stanford University, Stanford, CA, 1968), pp. 47–54.

[11]L. P. Purtell, P S. Klebanoff, and F. T. Buckley, Phys. Fluids **24**, 802 (1981).

[12]D. E. Coles, Rand Report R-403-PR, 1962.

[13]F. M. White, *Viscous Fluid Flow* (McGraw–Hill, New York, 1974), pp. 500–502.

[14]N. K. Madavan, C. L. Merkle, and S. Deutsch, to be presented at ASME Fluids Engineering Conference, New Orleans, LA, February 1984.

[15]C. G. Koop, AIAA J. **13**, 683 (1975).

[16]C. E. Woolridge and R. J. Muzzy, AIAA J. **4**, 7009 (1966).

[17]J. L. Lumley, Phys. Fluids **20**, S64 (1977).

[18]J. L. Lumley, J. Polymer Sci., Macromol. Rev. **7**, 263 (1973).